

2-22

Copy 275
RM E51B13

NACA RM E51B13

E 51 B 13

TECH LIBRARY KAFB, NM
0143641

~~CONFIDENTIAL~~
NACA

RESEARCH MEMORANDUM

THEORETICAL AND EXPERIMENTAL INVESTIGATION
OF ADDITIVE DRAG

By Merwin Sibulkin

Lewis Flight Propulsion Laboratory
Cleveland, Ohio

Classification cancelled (or changed to *UNCLASSIFIED*)

By Authority of *NASA Tech Pub Announcement #16*
(OFFICER AUTHORIZED TO CHANGE)

By *[Signature]* *31 Jul 53*
NAME AND

GRADE OF OFFICER MAKING CHANGE

12 Apr 51 CLASSIFIED DOCUMENT

~~CONFIDENTIAL~~
This report contains information affecting the National Defense of the United States within the meaning of the Espionage Laws, Title 18, U.S.C. 50-51 and 52. Its transmission or the revelation of its contents in any manner to an unauthorized person is prohibited by law.
Information on this report should not be disseminated to the military and naval services of the United States, appropriate civilian agencies, or to the press, radio, television, or any other public medium, without the approval of the person or office to whom this report is submitted, and to United States citizens of known loyalty.

NATIONAL ADVISORY COMMITTEE FOR AERONAUTICS

WASHINGTON

May 21, 1951

~~CONFIDENTIAL~~

8599

319.98/13

NATIONAL ADVISORY COMMITTEE FOR AERONAUTICS

RESEARCH MEMORANDUM

THEORETICAL AND EXPERIMENTAL INVESTIGATION OF ADDITIVE DRAG

By Merwin Sibulkin

SUMMARY

2112
6112

The significance of additive drag is discussed and equations for determining its approximate value are derived for annular- and open-nose inlets. Charts are presented giving values of additive drag coefficient over a range of free-stream Mach numbers for open- and for annular-nose inlets with conical flow at the inlet. The effects on additive drag of variable inlet-total-pressure recovery and static pressures on the center body are investigated and an analytical method of predicting the variation of pressure on the center body with mass-flow ratio is given.

Experimental additive-drag values are presented for a series of 20° and 25° cone half-angle inlets and one open-nose inlet operating at free-stream Mach numbers of 1.8 and 1.6. A comparison with the theoretical values of additive drag shows excellent agreement for the open-nose inlet and moderately good agreement for the annular inlets.

INTRODUCTION

In the analysis of engine performance it has been customary to define a net-thrust term that is evaluated between the outlet of the engine and a station ahead of the engine where the entering stream tube is at free-stream conditions. If the area of the entering stream tube at free-stream conditions is not equal to the inlet area, conditions at the inlet differ from those in the free stream and if the flight velocity is supersonic, an additional force must be considered in determining the net propulsive thrust. This additional force has been called additive drag (reference 1). At subsonic flight velocities, however, this additional force is approximately counterbalanced by a decrease in the engine nacelle pressure drag and, consequently, it has not been customary, when considering subsonic aircraft, to break down engine nacelle drag into its component parts.

A theoretical method of predicting the magnitude of the additive drag at supersonic speeds that is based upon an analysis of the location

PERMANENT
RECORD

of detached shock waves as a function of relative mass flow and Mach number is included in reference 2, and a method based upon an analysis of the entering stream tube is included in reference 3. For configurations having side inlets, an analysis of the effect of changes in the entering air conditions ahead of the inlet is given in reference 4. A method of determining the sum of additive and cowl-pressure drags from an analysis of the external shock configuration is presented in reference 5. Some experimental values of additive drag at Mach numbers from 1.35 to 2.0 are given in references 6 to 8.

In this report, the necessity for including the effect of additive drag in calculating the net propulsive thrust is discussed and a modified method of predicting the additive drag is presented. Theoretical values calculated by the modified method are compared with the values predicted by the methods given in references 2 and 3 and with experimental values of additive drag obtained from tests of ram jets in the 8- by 6-foot supersonic tunnel. Experimental values of additive drag, obtained using the method of reference 5, are compared with values obtained from pressure measurements.

SYMBOLS

The following symbols are used in this report:

A	flow area, (sq ft)
A_c	capture area, cross-sectional area at cowl lip including center-body area, (sq ft)
A_s	cross-sectional area of center body at station 1, (sq ft)
A_x	component of surface area perpendicular to longitudinal axis of inlet, (sq ft)
A_y	area of center body where it is intersected by bow wave, (sq ft)
$C_{d,a}$	additive-drag coefficient, $2D_a/\rho_0 V_0^2 A_c$
$C_{f,s}$	friction-force coefficient on center body, $2F_{f,s}/\rho_0 V_0^2 A_c$
C_s	incremental-cone-pressure coefficient, $2A_s(\bar{p}_s - p_c)/\rho_0 V_0^2 A_c$
D_a	additive drag, (lb)

F	total momentum, $mV + A(p - p_0)$, (lb)
F_d	sum of external pressure and friction drags, (lb)
$F_{f,s}$	axial component of force on fluid due to friction on portion of center body forward of station 1, (lb)
F_j	jet thrust, $mV_e + A_e(p_e - p_0)$, (lb)
F_n	net thrust, (lb)
$F_{n,i}$	net internal thrust, (lb)
F_p	inertial reaction of net propulsive thrust, (lb)
F_s	scoop incremental drag, (lb)
g	acceleration due to gravity, (ft/sec ²)
K	bow-wave-position parameter
M	Mach number
m	mass-flow rate of fluid passing through inlet, (slugs/sec)
m_{max}	maximum theoretical rate of mass flow through capture area $\equiv \rho_0 V_0 A_c$, (slugs/sec)
P	total pressure, (lb/sq ft absolute)
p	static pressure, (lb/sq ft absolute)
P_c	theoretical static pressure on surface of cone behind an oblique shock, (lb/sq ft absolute)
\bar{P}_s	effective static pressure on portion of center body forward of station 1, (lb/sq ft absolute)
P_w	theoretical static pressure immediately behind an oblique shock wave, (lb/sq ft absolute)
R	gas constant, (ft/°R)
T	total temperature, (°R)

- t static temperature, ($^{\circ}$ R)
- V velocity, (ft/sec)
- β ratio of mass-flow rate with supersonic flow at inlet to maximum theoretical capture-area mass flow
- γ ratio of specific heats
- θ_c cone half-angle of inlet center body
- θ_2 cowl-position parameter, angle between axis of inlet and straight line that connects tip of center body with lip of cowl
- λ angle at station 1 between average direction of flow and longitudinal axis of inlet
- ρ density, (slugs/cu ft)

Subscripts:

- 0 free stream
- 1 conditions at engine inlet (defined in text for particular types of inlet)
- e conditions at engine outlet

ANALYSIS

The net propulsive thrust of an engine at zero angle of attack is the resultant of the sum of the axial components of the pressure and friction forces acting on the engine. A schematic representation of these forces as applied to a ram jet in accelerated flight is shown in figure 1, in which the net propulsive thrust of the engine is replaced by an equal and opposite inertial force F_p according to D'Alembert's principle for accelerating systems. The forces are defined as positive in the directions shown by their arrows.

The sum of pressure and friction forces acting on the interior of the engine, which is called the net internal thrust $F_{n,1}$, can be calculated from the change in total momentum $mV + A(p - p_0)$ between stations 1 and e of the fluid passing through the engine (fig. 1(a)), that is,

$$F_{n,i} = F_j - F_1 \quad (1)$$

where $F_j \equiv mV_e + A_e(p_e - p_0)$ and $F_1 \equiv mV_1 + A_1(p_1 - p_0)$.

Then

$$F_p = F_{n,i} - F_d \quad (2)$$

where F_d is the sum of the pressure and friction forces acting on the exterior of the engine.

It is customary, however, to evaluate engine performance between stations 0 and e (fig. 1(b)) and to call the change in total momentum of the internal flow (between stations 0 and e) the net thrust F_n as given by

$$F_n = F_j - F_0 \quad (3)$$

where

$$F_0 \equiv mV_0 + A_0(p_0 - p_0) = mV_0$$

In this case, however,

$$F_p \neq F_n - F_d$$

because the change in total momentum of the free stream between stations 0 and 1 has not been considered. Therefore, in order to obtain the net propulsive thrust F_p , this momentum change (which is called additive drag D_a) must be included to give

$$F_p = F_n - F_d - D_a \quad (4)$$

A mathematical definition of additive drag can be obtained by combining equations (1) to (4) to give

$$D_a = F_n - F_{n,i} = F_1 - F_0 \quad (5)$$

or using the definitions of F_1 and F_0

$$D_a = mV_1 + A_1(p_1 - p_0) - mV_0 \quad (5a)$$

where appropriate average values of the quantities at station 1 are used.

Another interpretation (which gives physical meaning to net thrust F_n) is to consider that the diverging portion of the entering stream tube behind a bow wave (fig. 2(a)) from I to II is replaced by a thin, frictionless membrane (fig. 2(b)). Inasmuch as the flow field is unchanged, the net propulsive thrust F_p will not be affected. Because the engine has already been credited with the thrust due to the pressure acting on the interior of the hypothetical extension of the engine from I to II by its inclusion in the net thrust F_n , a drag force must be added because of the pressure acting on the exterior of the engine extension which is equal to

$$\int_I^{II} (p - p_0) dA_x$$

where dA_x is the axial projection of the surface area. This integral may also be used to define the additive drag and is equivalent to the definition given by equation (5a), as can easily be seen by applying the momentum theorem around the surface I,II,III,IV,I in figure 2(b).

Although no change in the forces on the inlet occurs when an inlet is extended to free-stream diameter along a streamline, an increase in net propulsive thrust would be obtained if the inlet were extended in the manner shown in figure 2(c). In this case the angle through which the entering streamline is turned is made smaller than the detachment angle and the bow wave is replaced by a normal shock at the entrance to the inlet and an oblique shock off the lip. Comparing the modified inlet in figure 2(c) with the one in figure 2(a), it has been found that the increase in the cowl-pressure drag owing to the extension of the inlet from II to I is much less than the value of the additive drag eliminated because the increase in pressure behind the oblique shock in figure 2(c) is much less than the pressure rise behind the nearly normal shock in figure 2(a).

Equation (5a) applies directly only to an open-nose inlet. The comparable equation for an annular-nose inlet can be derived by considering the forces acting on the surface bounded by I,II,III,IV,V,I as shown in figure 3(a). A summation of the axial components of the forces acting on the enclosed fluid gives

$$D_a = mV_1 \cos \lambda + A_1 \cos \lambda (p_1 - p_0) + A_s (\bar{p}_s - p_0) - mV_0 + F_{f,s} \quad (5b)$$

where A_1 corresponds to the flow area II, III, and $A_s(\bar{p}_s - p_0)$ and $F_{f,s}$ are, respectively, the axial components of the pressure and the friction forces acting on the center body, and appropriate average values are used at station 1 and on the center body. Again, as in the case of the open-nose inlet, a definition of additive drag equivalent to equation (5b) is

$$D_a = \int_I^{II} (p - p_0) dA_x$$

A side- or scoop-type inlet can be considered to be an annular-nose inlet with the center body greatly extended (fig. 3(b)) and consequently its additive drag can be found from equation (5b).

If, however, the scoop does not extend completely around the center body, it is extremely difficult to determine the portion of the center body which forms part of the boundary of the entering stream tube (indicated by shaded surface on diagram) and, consequently, to determine the proper value of A_s for use in equation (5b). Furthermore, for this type of fuselage, the drag on the shaded portion of the center body is customarily included in the body drag. Consequently, it has been suggested in reference 4, that if the approximation be made that the drag on the shaded portion of the center body does not change as the mass flow through the engine changes, then a scoop incremental drag F_s can be defined equal to the change in total momentum of the entering stream tube between station 0 and 1; that is,

$$F_s = mV_1 \cos \lambda + A_1(p_1 - p_0) - mV_0 \quad (5c)$$

Then

$$F_p = F_n - F_d - F_s$$

where F_d includes the drag on the shaded portion of the center body.

If the direction of flow at station 1 is parallel to the axis, the formulas for evaluating the scoop incremental drag and the additive drag of an open-nose inlet (equation (5a)) are the same.

~~CONFIDENTIAL~~

APPARATUS AND PROCEDURE

Experimental values of additive drag were obtained in the NACA Lewis 8- by 6-foot supersonic tunnel for one open-nose and several annular-nose inlets. The inlets formed the forward end of a 16-inch ram jet, which is schematically shown in figure 4. Two cone angles were tested; the projection of the center bodies was varied by cylindrical spacer blocks so as to obtain various supercritical mass-flow ratios. The values of cone angle, center-body position, and design mass-flow ratio investigated are given in the table appearing in figure 4.

Tests were conducted at free-stream Mach numbers of 1.8 and 1.6 over a range of mass-flow ratio, which was controlled by a variable-area orifice valve located in the engine combustion chamber. Static pressures on the internal surface of the cowl and on the center body forward of station 2 (located 15 in. back of cowl lip) were measured by wall orifices and total pressure at station 2 was measured by a rake of total-pressure tubes. The weight flow was calculated from the total- and static-pressure readings at station 2 and a correction factor was applied to bring the data in agreement with the theoretical values of supercritical mass flow. The additive drag was then calculated by taking a momentum balance around the surface I, II, III, IV, V, VI, I of figure 4.

COMPARISON OF THEORY AND EXPERIMENT

Open-Nose Inlets

The equation for the additive-drag coefficient $C_{d,a}$ for an open-nose inlet based on the inlet lip area may be derived from equation (5a) as shown in the appendix to give

$$C_{d,a} = \frac{2}{\gamma M_0^2} \left[\frac{P_0}{P_0} \frac{P_1}{P_0} \frac{P_1}{P_1} (\gamma M_1^2 + 1) - 1 - \frac{A_0}{A_1} \gamma M_0^2 \right] \quad (6)$$

where

$$\frac{A_0}{A_1} = \frac{\rho_0 V_0 A_0}{\rho_0 V_0 A_1} = \frac{m}{m_{\max}}$$

For given values of M_0 and mass-flow ratio, the value of M_1 can be obtained by applying the continuity equation between stations 0 and 1. This relation may be written in the form

$$\frac{A_0}{A_1} f(M_0) = f(M_1) \frac{P_1}{P_0} \quad (7)$$

where

$$f(M) = M \left(1 + \frac{\gamma-1}{2} M^2 \right)^{-\frac{\gamma+1}{2(\gamma-1)}}$$

with the usual assumption that $T_1 = T_0$. The pressure ratio P_1/P_0 is taken equal to the value across a normal shock occurring at M_0 . Inasmuch as p_1/P_1 and p_0/P_0 are known functions of M_1 and M_0 , all the quantities in equation (6) are determined.

The values of additive-drag coefficient for an open-nose inlet operating at Mach numbers from 1.2 to ∞ have been calculated by the foregoing procedure and are presented in figure 5. For a fixed value of mass-flow ratio m/m_{\max} , the value of $C_{d,a}$ increases with increasing M_0 and approaches a finite limit for $M_0 = \infty$.

A comparison of theoretical (predicted by equation (6)) and experimental (fig. 6) values of additive drag at $M_0 = 1.8$ and 1.6 indicates good agreement down to $m/m_{\max} \approx 0.4$, the lowest mass-flow ratio investigated. Because the additive drag of an open-nose inlet at a mass-flow ratio of 1.0 must equal zero, the discrepancies at that point can be attributed to errors in the experimental analysis. Part of this discrepancy is caused by the omission of the unknown force resulting from friction on the inside of the cowl forward of station 2 in calculating the experimental values of additive-drag coefficient. Curves of the additive drag coefficient predicted by the theory of reference 2 are also shown. This theory predicts a linear variation of additive drag with mass-flow ratio that agrees with the present analysis at mass-flow ratios near 1.0, but underestimates the additive drag at lower mass-flow ratios.

Annular-Nose Inlets

Before discussing the additive drag of annular-nose inlets, a basic difference between annular- and open-nose inlets should be considered. When an open-nose inlet is operating without a bow wave, the mass-flow ratio m/m_{\max} must equal 1.0 and consequently the additive drag must equal zero. For an annular-nose inlet, however, the mass-flow ratio as herein defined will not equal 1.0 even when no bow wave is present

~~CONFIDENTIAL~~

unless the oblique shock stands at or inside the cowl lip. If the oblique shock stands upstream of the cowl lip, it follows that, owing to the change in area of the entering stream tube behind the oblique shock the mass-flow ratio is less than 1.0 and the additive drag is greater than zero. Consequently, it is useful to define an annular-inlet parameter β equal to the ratio of mass-flow rate with supersonic flow at the inlet to the maximum theoretical capture-area mass flow. For most cases this definition is equivalent to defining β as the supercritical mass-flow ratio. Because from its definition the parameter β is a function only of M_0 and of the geometry of the inlet, an inlet having a value of $\beta = 1.0$ at the design M_0 has a value of $\beta < 1.0$ at an M_0 below design.

Operation with conical flow at inlet. - When an annular-nose inlet having a center body that is conical forward of station 1 (fig. 3(a)) is operating without any bow waves, the flow behind the oblique shock generated by the center body can be predicted from conical flow theory (for example, reference 9). In this case it is possible to evaluate the

additive drag directly from $\int_I^{II} (p - p_0) dA_x$. This procedure has been

followed for four cone angles over a range of Mach numbers from a value slightly greater than the minimum for an attached shock to an M_0 of 5.0 (fig. 7). The curves show that for a fixed value of mass-flow ratio, the additive-drag coefficient decreases as M_0 increases, which is opposite to the trend in figure 5 for an open-nose inlet. The variation of values of mass-flow ratio with cowl-position parameter θ_1 is also given from which the theoretical supercritical mass-flow ratio β can be determined when the geometry of the inlet and M_0 are known.

Operation with bow wave. - The equation for the additive-drag coefficient based on the capture area A_c of an annular-nose inlet can be derived from equation (5b) (as shown in the appendix) to give

$$C_{d,a} = \frac{2}{\gamma M_0^2} \left[\frac{A_1}{A_c} \frac{P_0}{P_0} \frac{P_1}{P_0} \frac{P_1}{P_1} (\gamma M_1^2 + 1) \cos \lambda + \frac{A_s \bar{P}_s}{A_c P_0} - 1 - \frac{A_0}{A_c} \gamma M_0^2 \right] + C_{f,s} \quad (8)$$

where appropriate average values are used at station 1.

In evaluating equation (8), M_1 can be found by applying the continuity equation (equation (7)) as a function of $A_0/A_c = (A_0/A_1)(A_1/A_c)$ if the average pressure recovery P_1/P_0 and flow angle λ are known. For calculations involving an inlet having a center body that is conical

~~CONFIDENTIAL~~

forward of station 1, when the oblique shock stands at the lip ($\beta = 1.0$), the pressure recovery P_1/P_0 is closely approximated by the product of the pressure ratio across an oblique shock and the ratio across a normal shock occurring at the average of the Mach numbers on the cone surface and directly behind the oblique shock. If it is assumed that the average flow angle λ is independent of β , λ can be determined for an inlet whose β equals 1.0 by the condition that $C_{d,a} = 0$ for $m/m_{\max} = 1.0$. The effect of friction on the center body $C_{f,s}$ is negligible and can be assumed to be zero.

In reference 3, it was assumed as a first approximation that $\bar{P}_s/P_0 = P_c/P_0$. This assumption will give the correct value of additive drag when the mass-flow ratio equals β , and should increasingly underestimate the additive drag as the mass-flow ratio is reduced. It was also assumed that for subcritical flow the value of pressure recovery was constant at the value previously described for $\beta = 1.0$. The assumptions described previously for P_1/P_0 , \bar{P}_s/P_0 , λ , and $C_{f,s}$ have been used in obtaining the theoretical additive-drag curves in references 7 and 8. An improved approximation for \bar{P}_s/P_0 , and the effect of variations in the pressure recovery from the value assumed are discussed in the following sections:

Prediction of pressures on center body. - A better approximation for \bar{P}_s/P_0 can be based upon a simplification of the results given in reference 2 for determining the position of a bow wave. In terms of the notation given on the sketch in figure 8, calculations based upon equations in reference 2 show that for an annular-nose inlet with $\beta \approx 1.0$, the variation of L'/y_c with mass-flow ratio is approximately linear for $M_0 \geq 1.6$. The length y_c is the radius of the inlet at the cowl lip, and the assumption is made that $L = L'$, where L is the axial distance from the point where A_s is measured to the point where the bow wave intersects the center body. As a simplification it will be assumed that $L/y_c = K(1 - m/m_{\max})$; K is independent of cone angle and its variation with M_0 is given in the following table:

M_0	1.6	2.0	2.4	2.8	3.2
K	1.13	.89	.76	.69	.65

The values of K were determined by plotting L/y_c against mass-flow ratio and finding the mean slope of the curves. Then from the geometry of the figure

$$y = y_s - y_c K (1 - m/m_{\max}) \tan \theta_c$$

~~CONFIDENTIAL~~

where y_g is the radius at A_g . This gives

$$\frac{A_y}{A_c} = \left[\sqrt{\frac{A_g}{A_c}} - K(1 - m/m_{\max}) \tan \theta_c \right]^2 \quad (9)$$

from which A_y can be calculated.

Forward of A_y , the pressure on the center body equals the previously assumed value of p_c . The average pressure \bar{p} behind A_y will lie between p_1 and p_y , defined as the value behind a normal shock at the cone surface Mach number; it will be assumed that $\bar{p} = (p_y + p_1)/2$. An incremental-cone-pressure coefficient $C_s \equiv 2A_g(\bar{p}_s - p_c)/\rho_0 V_0^2 A_c$ can now be defined. When added directly to the value of $C_{d,a}$ obtained using the approximation $\bar{p}_s = p_c$, C_s will account for the increase in additive drag caused by the increase of pressure on the cone behind the bow wave. Using the development given

$$C_s = \frac{2}{\gamma M_0^2} \frac{(A_g - A_y)}{A_c} \frac{(\bar{p} - p_c)}{p_0} \quad (10)$$

The variation of C_s with mass-flow ratio for a 25° half-angle cone is shown in figure 8 for a range of M_0 .

Although the approximate relation $L/y_c = K(1 - m/m_{\max})$ is based upon a derivation in reference 2 for inlets with $\beta \approx 1$, it will be assumed that for other inlets the relation $L/y_c = K [1 - (m/m_{\max})(1/\beta)]$ is approximately true, where the values of K are the same as those given previously. Using this approximation a comparison of the variation of the theoretical and experimental values of C_s with $(m/m_{\max})(1/\beta)$, is shown in figure 9. For a given M_0 at a fixed value of $(m/m_{\max})(1/\beta)$, the theory predicts that C_s increases as β decreases. The scatter of the experimental data is, however, too great to allow a conclusion to be drawn as to the variation of C_s with β for the inlets tested. For mass-flow ratios less than approximately 0.85 to 0.95, the flow into the inlets was pulsating so that the model upon which the theoretical results are based can only be considered to represent an average condition and scatter in the data is to be expected. Nevertheless, for $\theta_c = 20^\circ$, the theory agrees with the data moderately

~~CONFIDENTIAL~~

2119

well; for $\theta_c = 25^\circ$, the experimental values are greater than theoretical. In all cases the theory is an improvement over the previous assumption, which corresponds to $C_s = 0$.

The variation of additive-drag coefficient with mass-flow ratio as calculated from equation (8) including the effect of the incremental-cone-pressure coefficient C_s and using the value of pressure recovery P_1/P_0 , described previously for $\beta = 1.0$, is shown in figure 10 at three values of β for each of two annular inlets operating at $M_0 = 1.8$. For comparison, the value of additive-drag coefficient for an open-nose inlet at the same M_0 is also shown. For a fixed value of mass-flow ratio and as β decreases from 1.0, the additive drag decreases from a value greater than that for an open-nose inlet to a minimum when the flow at the inlet is supersonic. Curves of the minimum value of $C_{d,a}$, as determined from equation (8) which is obtainable at each value of mass-flow ratio (that is, when the flow at the inlet is supersonic), are also shown for both cone angles. Comparable curves computed from conical flow theory (fig. 7) are shown for comparison. The differences in these minimum additive-drag curves can be attributed to the small changes in pressure recovery and flow angle λ that occur as β is reduced and which were neglected in the evaluation of equation (8). Each point on these minimum $C_{d,a}$ curves corresponds to a different inlet configuration, whereas the curves for a given β refer to one inlet. From figure 10, if a given amount of air must be spilled it is better, from additive drag considerations, to achieve this by allowing the oblique shock to stand upstream of the cowl lip rather than by spilling the air behind a bow wave. Consequently, for an engine designed to operate over a range of M_0 , an appreciable gain in net propulsive thrust can be realized at values of M_0 below the design value by utilizing an inlet in which the projection of the center body increases as M_0 decreases to maintain supersonic flow at the inlet

Effect of inlet total-pressure recovery. - The additive-drag curves of figure 10 assume that the pressure recovery P_1/P_0 is constant at the value calculated for $\beta = 1.0$. The experimental total-pressure ratio between stations 0 and 2 is shown in figure 11 and compared to the assumed value of P_1/P_0 . If it is assumed that P_2/P_1 is very close to 1.0, the difference between the experimental and theoretical values indicates that the effect on additive drag of a reduction in pressure recovery should be considered. The effect on additive drag of varying the ratio of assumed pressure recovery to the recovery for $\beta = 1.0$ from 1.0 to 0.8 at two values of β for an annular inlet with a 20° half-angle cone at $M_0 = 1.8$ is shown in figure 12. Overestimating the pressure

recovery overestimates the additive drag by an amount that is independent of mass-flow ratio for a given value of β but decreases as β decreases.

Experimental values of additive drag obtained from tests of annular-nose inlets are shown in figure 13 for free-stream Mach numbers of 1.8 (design value) and 1.6. These results are compared with the theoretical curves obtained from equation (8) using the approximations of reference 3 and using the approximation for \bar{p}_s/p_0 presented in this paper and experimental values of pressure recovery. The curves calculated with the present method also begin at the more exact values of additive-drag coefficient given in figure 7.

The discrepancies between the experimental data and the theoretical curves of the present method at and near supercritical flow conditions can be attributed primarily to the omission of the unknown force due to friction on the center body and cowl forward of station 2 in calculating the experimental values of additive-drag coefficient. This error is greatest near supercritical flow conditions and decreases as the mass-flow ratio decreases. At lower values of mass-flow ratio, the differences between theory and experiment are due primarily to the error made in predicting the magnitude of the force resulting from the variable static pressures on the center body, as can be seen by comparing the differences between theory and experiment in figures 9 and 13. As previously suggested, these errors may be due in part to the pulsating condition of the flow at low mass-flow ratios.

The good agreement shown here between the experimental data for inlets with $\beta \approx 1$ and the theoretical curves obtained using the assumptions of reference 3 (which was also obtained in references 7 and 8) is due to a fortuitous cancellation of the errors due to assuming higher pressure recoveries and lower pressures on the center body than those actually obtained.

CALCULATION OF ADDITIVE DRAG FROM SCHLIEREN PHOTOGRAPHS

Another means of calculating additive drag, which approaches the problem from a different viewpoint, can be obtained from the method presented in reference 5. This method allows the sum of the additive and cowl-pressure drags to be computed using a schlieren photograph of the inlet shock configuration and knowing the mass-flow ratio m/m_{\max} . If the cowl-pressure drag can be determined by another method, subtracting it from the sum of the two drags will give the additive drag. The method involves taking a momentum balance around the surface

I,II,III,III',IV,V,VI,I as shown in figure 14, where it is assumed that the cowl is cylindrically extended downstream from its point of maximum diameter III, to station X so that $p_X = p_0$ and $A_{III'} = A_{III}$. An arbitrary point V on the bow wave is then chosen and the streamline VI,V,IV extended through it. Then

$$\int_{III}^{III'} (p - p_0) dA_X = m(V_0 - V_X) + (\bar{p}_{IV,V} - p_0) (A_{IV} - A_V) \quad (11)$$

where $\int_{II}^{III'} (p - p_0) dA_X$ defines the sum of the additive and cowl-pressure drags. In reference 5 two alternative assumptions are suggested for $\bar{p}_{IV,V}$; namely, $\bar{p}_{IV,V} = p_w$ at V, which gives an upper limit, and $\bar{p}_{IV,V} = (p_w + p_0)/2$, which generally gives a lower limit. The flow is also assumed to be isentropic behind the bow wave.

In order to evaluate equation (11) it is necessary to determine m , V_X (or M_X), and A_{IV} . The mass flow m can be calculated from $\rho_0 V_0 (A_{VI} - A_I)$, where A_I is a function of the given mass-flow ratio. The total pressure behind the bow wave $\bar{p}_{II,V}$ can be determined by properly weighting the total-pressure loss across the bow wave at several points from II to V. Then from the isentropic flow assumption M_X can be determined from $p_0/\bar{p}_{II,V}$. Finally, A_{IV} can be computed by applying the continuity equation between stations 0 and X.

The results of such a calculation for additive-drag coefficient, using a shock length of two inlet diameters, are shown in figure 14 for an annular inlet with a 25° half-angle cone operating at $M_0 = 1.79$ and compared with values obtained from pressure measurements presented in reference 7. The cowl-pressure drag used in computing the curves was also taken from reference 7.

The curves show that for the shock length used the assumption made for $\bar{p}_{IV,V}$ greatly influences the results. For the engine tested, the assumption that $\bar{p}_{IV,V} = (p_w + p_0)/2$ gave good agreement, especially at high mass-flow ratios. In order to determine the importance of accurately determining the average pressure ratio across the portion of the bow wave considered, the effect on the values of additive drag of an

error of 0.5 percent in $\bar{P}_{II,V}$ was also calculated (by multiplying the computed $\bar{P}_{II,V}$ by 0.995) and is shown for each assumption of $\bar{P}_{IV,V}$; the effect is relatively small

SUMMARY OF RESULTS

Formulas were developed for determining the additive drag of annular- and open-nose inlets. Calculations based upon these formulas showed that for a fixed lip area and cone angle the additive drag at a given mass-flow ratio varied with the projection of the center body and was least when the flow at the inlet was supersonic.

The effect on additive drag of changes in the free-stream Mach number was relatively small. For annular inlets, the additive drag decreased with increasing Mach number when the flow at the inlet was supersonic but increased with increasing Mach number for most cases when there was a bow wave ahead of the inlet. For open-nose inlets, the additive drag increased with increasing Mach number.

The forces due to the variation of static pressure on the center body with mass-flow ratio were considered, and an analytical method of approximating their value was developed which showed that they represented an appreciable portion of the additive drag. Overestimating the inlet total-pressure recovery resulted in an estimate of additive drag that was too large.

Comparisons of the theoretical values of additive drag with experimental results showed excellent agreement for an open-nose inlet and moderate agreement for several annular-nose inlets when the effects of variable center body pressures and inlet pressure recovery were considered in obtaining the theoretical results.

Consideration of a proposed method of obtaining the external drag from schlieren photographs showed that when a shock length of two inlet diameters was used the results depended largely upon the value of one of the assumptions involved. For the particular configuration to which this method was applied, one of the suggested values for this assumption gave good agreement with the value of additive drag obtained from pressure measurements.

Lewis Flight Propulsion Laboratory,
National Advisory Committee for Aeronautics,
Cleveland, Ohio.

APPENDIX

DERIVATION OF ADDITIVE-DRAG COEFFICIENT $C_{d,a}$

FOR ANNULAR- AND OPEN-NOSE INLETS

The additive drag for an annular inlet is given in the text (equation (5b)) as

$$D_a = mV_1 \cos \lambda + A_1 \cos \lambda (p_1 - p_0) + A_s (\bar{p}_s - p_0) - mV_0 + F_{f,s} \quad (A1)$$

but it can be seen from figure 3(a) that

$$A_c = A_1 \cos \lambda + A_s$$

then

$$D_a = mV_1 \cos \lambda + A_1 p_1 \cos \lambda + A_s \bar{p}_s - A_c p_0 - mV_0 + F_{f,s} \quad (A2)$$

Substituting

$$m = \rho AV \quad \text{and} \quad \rho = p/gRt$$

gives

$$D_a = \frac{p_1 A_1 V_1^2 \cos \lambda}{gRt_1} \frac{\gamma}{\gamma} + A_1 p_1 \cos \lambda + A_s \bar{p}_s - A_c p_0 - \frac{p_0 A_0 V_0^2}{gRt_0} \frac{\gamma}{\gamma} + F_{f,s} \quad (A3)$$

Substituting $M^2 = V^2/\gamma gRt$ and dividing by $A_c p_0$ gives

$$\frac{D_a}{A_c p_0} = \frac{A_1 p_1 \gamma M_1^2 \cos \lambda}{A_c p_0} + \frac{A_1 p_1 \cos \lambda}{A_c p_0} + \frac{A_s \bar{p}_s}{A_c p_0} - 1 - \frac{A_0 \gamma M_0^2}{A_c} + \frac{F_{f,s}}{A_c p_0} \quad (A4)$$

Substituting $\frac{p_1}{p_0} = \frac{p_0}{p_0} \frac{p_1}{p_0} \frac{p_1}{p_1}$, rearranging, and converting into coefficient form gives

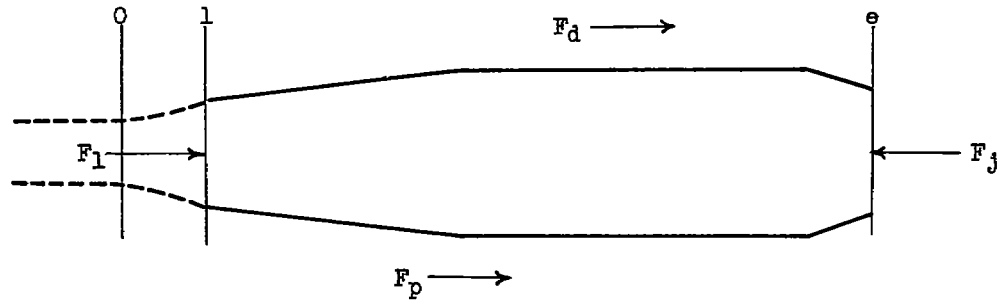
$$C_{d,a} = \frac{2}{\gamma M_0^2} \left[\frac{A_1}{A_c} \frac{p_0}{p_0} \frac{p_1}{p_0} \frac{p_1}{p_1} (\gamma M_1^2 + 1) \cos \lambda + \frac{A_s \bar{p}_s}{A_c p_0} - 1 - \frac{A_0}{A_c} \gamma M_0^2 \right] + C_{f,s} \quad (A5)$$

The value of $C_{d,a}$ for an open-nose inlet can be derived from equation (A5) by noting that for an open-nose inlet $A_1 = A_0$, $\cos \lambda = 1$, $A_s = 0$, and $C_{f,s} = 0$, which reduces equation (A5) to

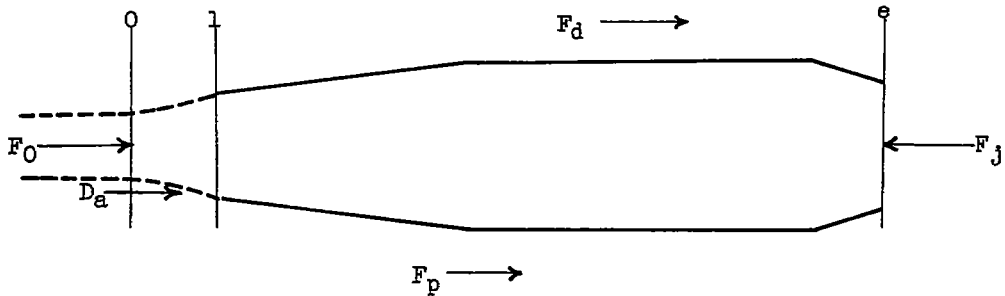
$$C_{d,a} = \frac{2}{\gamma M_0^2} \left[\frac{P_0}{P_0} \frac{P_1}{P_0} \frac{P_1}{P_1} (\gamma M_1^2 + 1) - 1 - \frac{A_0}{A_1} \gamma M_0^2 \right] \quad (A6)$$

REFERENCES

1. Ferri, Antonio, and Nucci, Louis M.: Preliminary Investigation of a New Type of Supersonic Inlet. NACA TN 2286, 1951.
2. Moeckel, W. E.: Approximate Method for Predicting Form and Location of Detached Shock Waves ahead of Plane or Axially Symmetric Bodies. NACA TN 1921, 1949.
3. Dailey, C. L., and McFarland, H. W.: Development of Ramjet Components. Prog. Rep. 9961-8, Aero. Lab., Univ. Southern Cal., Feb. 7, 1950. (Bi-Monthly Prog. Rep. Dec. 1949-Jan. 1950 under Navy Contract NOa(s)9961.)
4. Klein, Harold: The Calculation of the Scoop Drag for a General Configuration in a Supersonic Stream. Rep. No. S-13744, Douglas Aircraft Co., Inc., April 12, 1950.
5. Nucci, Louis M.: The External-Shock Drag of Supersonic Inlets Having Subsonic Entrance Flow. NACA RM L50G14a, 1950.
6. Perchonok, Eugene, and Farley, John M.: Internal Flow and Burning Characteristics of 16-Inch Ram Jet Operating in a Free Jet at Mach Numbers of 1.35 and 1.73. NACA RM E51C16, 1951.
7. Weinstein, Maynard I., and Davids, Joseph: Force and Pressure Characteristics for a Series of Nose Inlets at Mach Numbers from 1.59 to 1.99. III - Conical-Spike All-External-Compression Inlet with Supersonic Cowl Lip. NACA RM E50J30, 1951.
8. Nussdorfer, T., Wilcox, F., and Perchonok, E.: Investigation at Zero Angle of Attack of a 16-Inch Ram-Jet in the 8- by 6-Foot Supersonic Wind Tunnel. NACA RM E50L04, 1951.
9. Anon.: Tables of Supersonic Flow Around Cones. Vol. I., Dept. Elec. Eng., M.I.T., 1947.



(a) Using stations 1 and e.



(b) Using stations 0 and e.

Figure 1. - Schematic representation of forces acting on ram jet in accelerated flight.

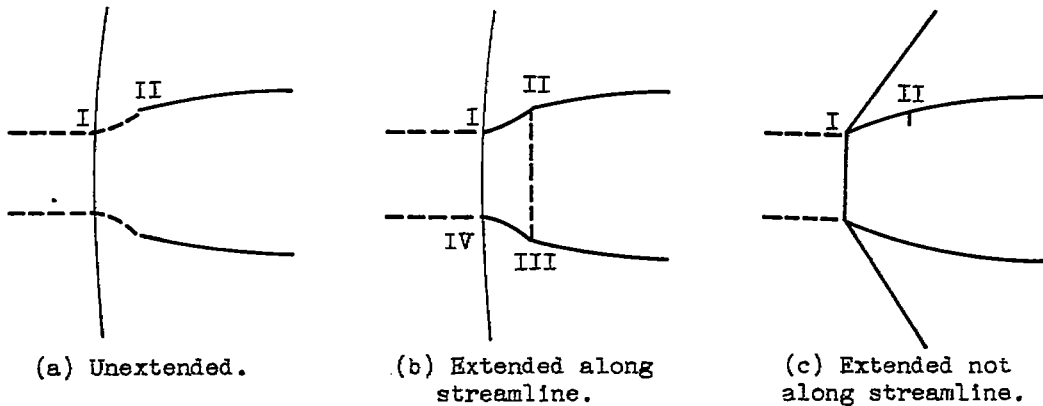
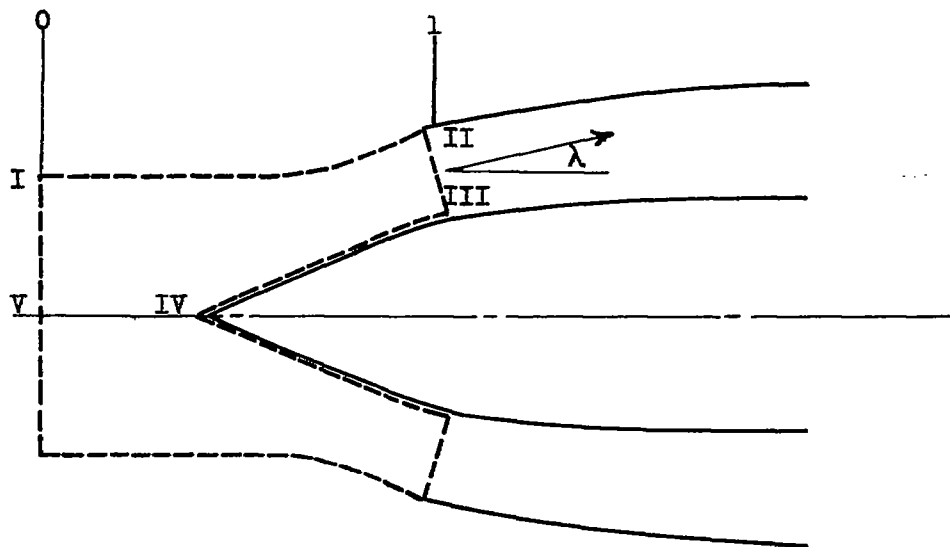
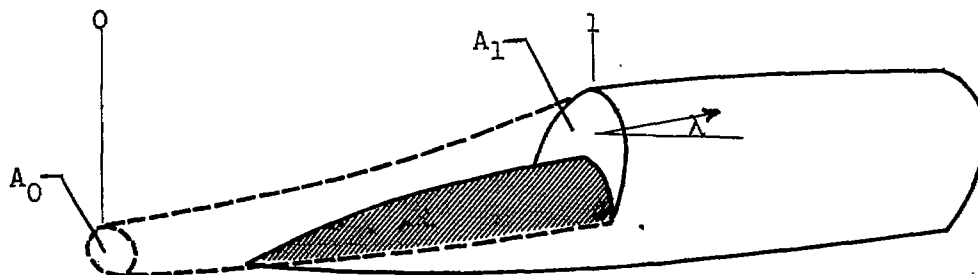


Figure 2. - Schematic representation of additive drag elimination by cowl extension.

CONFIDENTIAL



(a) Annular-nose inlet.

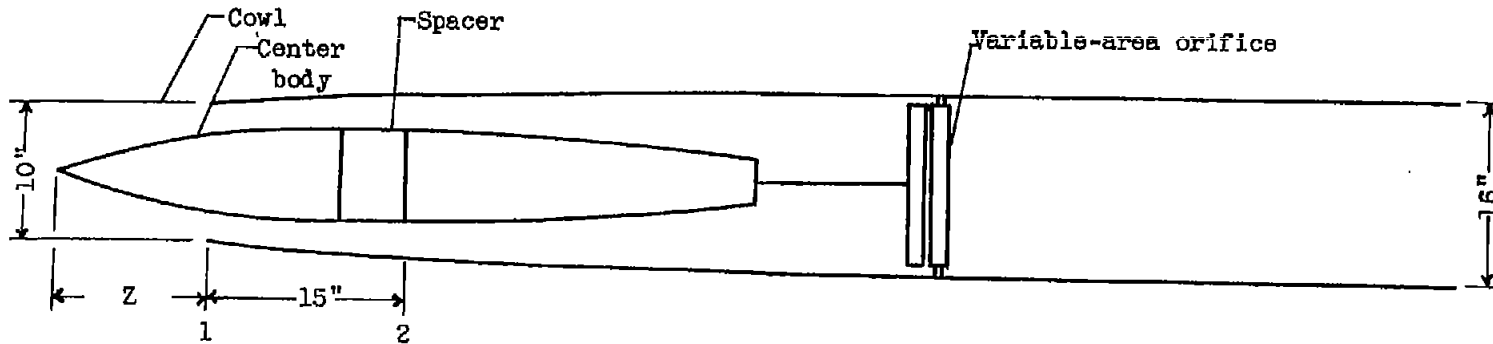


(b) Scoop inlet.

NACA

Figure 3. - Schematic views of annular-nose- and scoop-type inlets.

CONFIDENTIAL



Cone half-angle, (deg)	20	20	20	25	25	Open nose
Z, (in.)	5.63	8.47	10.47	6.71	8.21	----
Supercritical mass-flow ratio at $M_0 = 1.8$	1.0	0.75	0.51	0.75	0.51	1.0

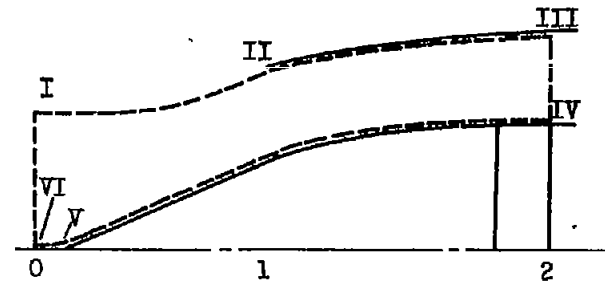


Figure 4. - Schematic diagram of inlet configurations investigated.



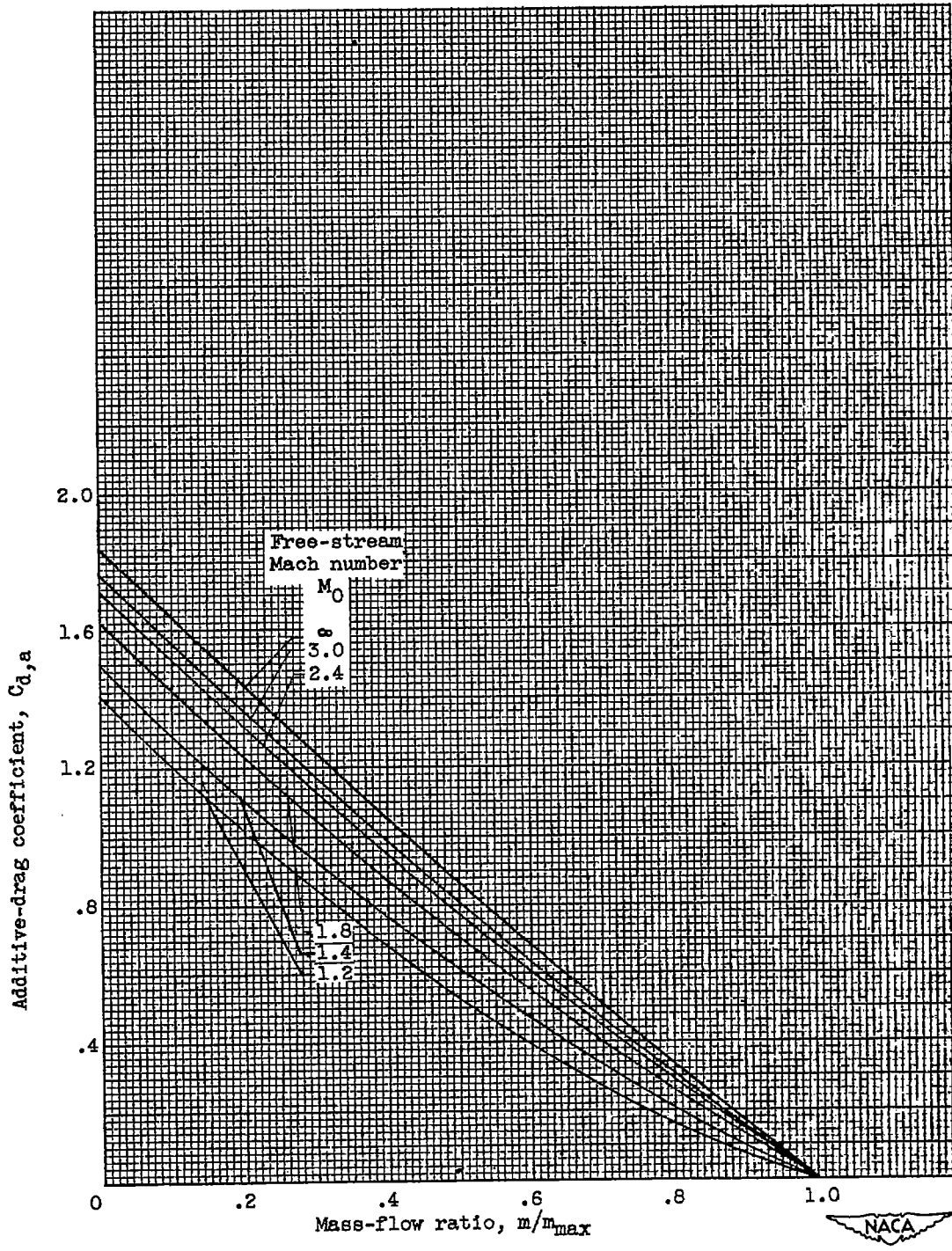
~~CONFIDENTIAL~~

Figure 5. - Variation of theoretical additive drag of open-nose inlet with free-stream Mach number.

~~CONFIDENTIAL~~

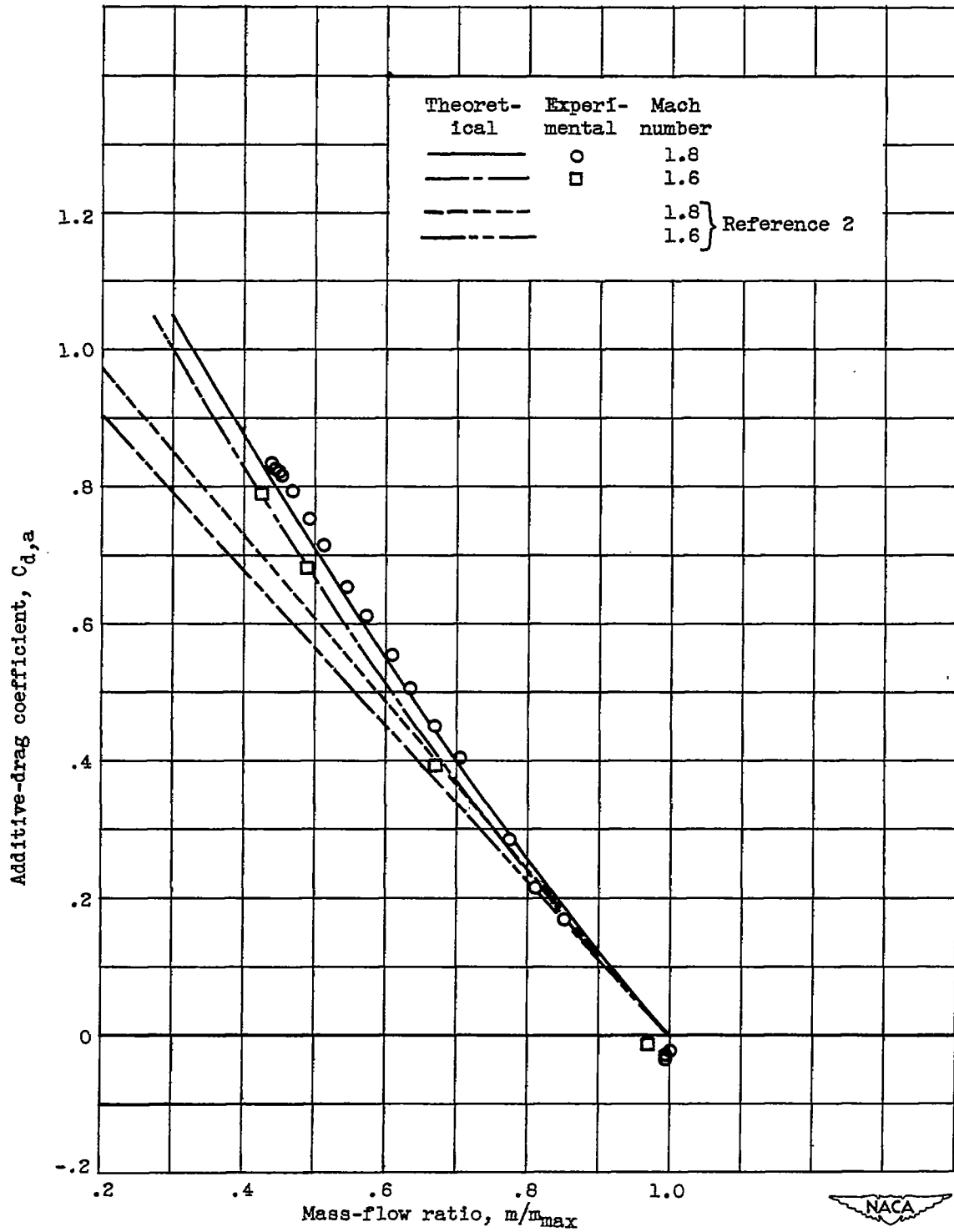


Figure 6. - Comparison of experimental and theoretical values of additive drag of open-nose inlet.

2119

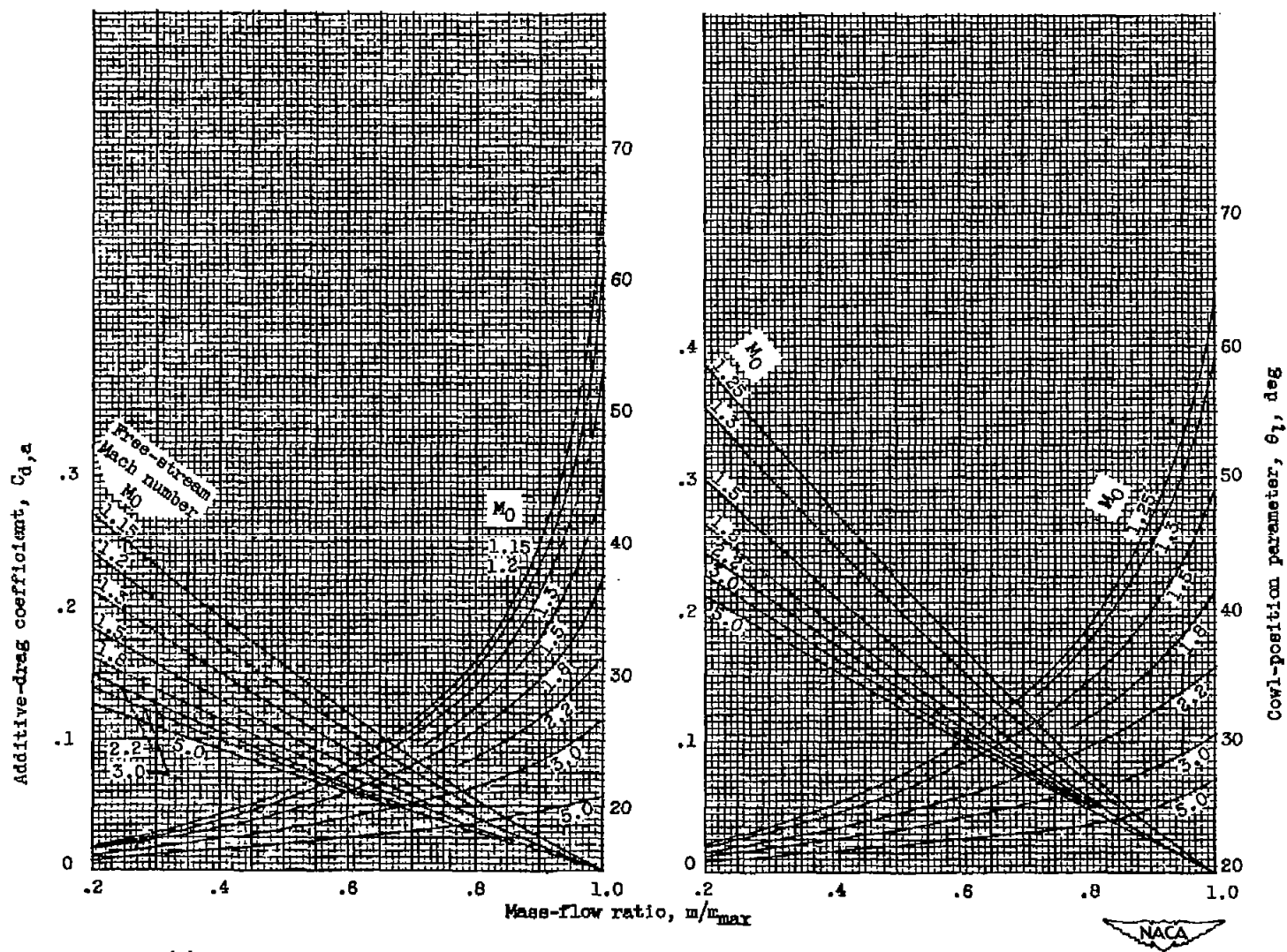
(a) Cone half-angle, 15° .(b) Cone half-angle, 20° .

Figure 7. - Variation of theoretical additive drag of annular-nose inlet with conical flow at inlet.

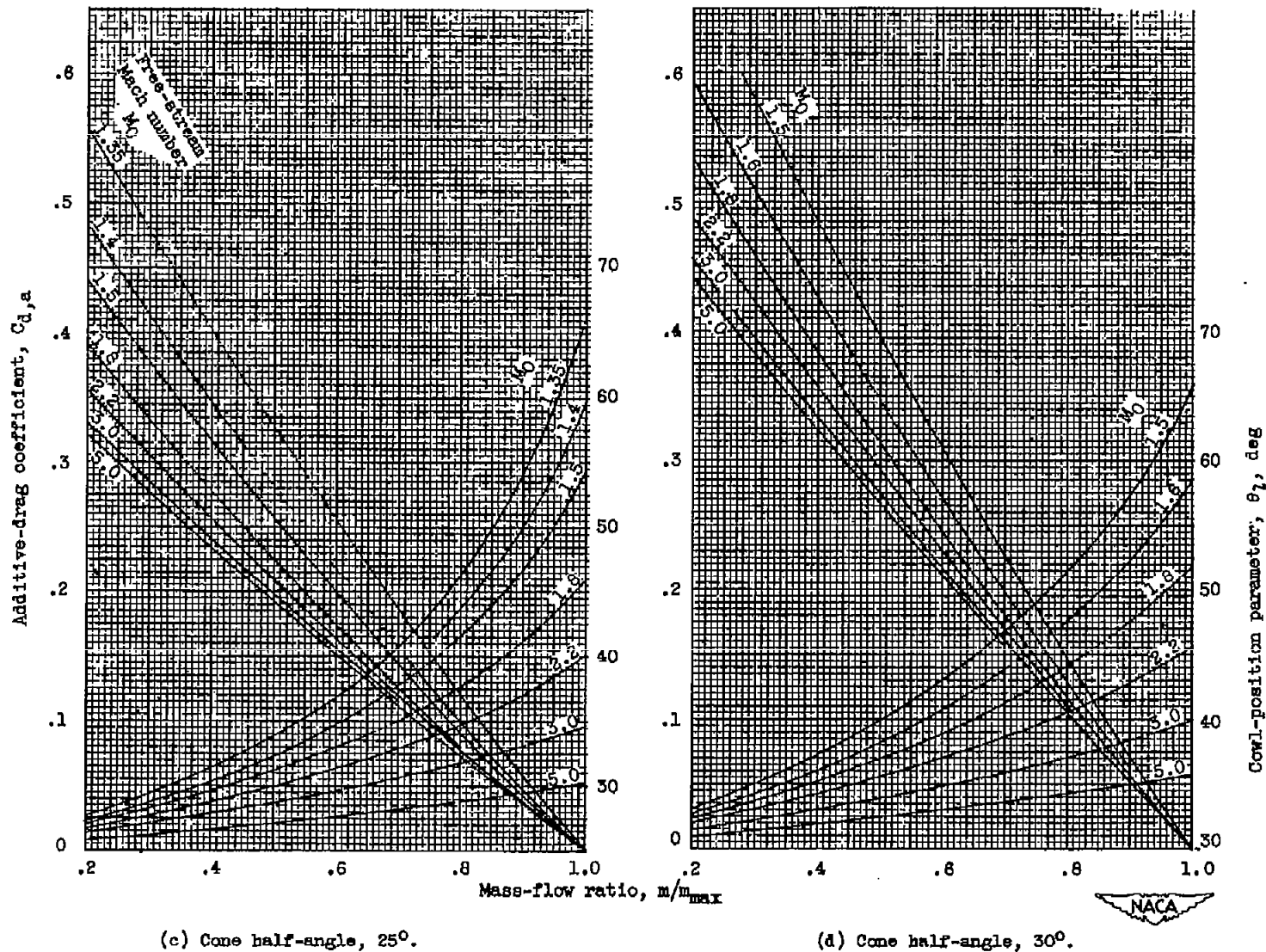
(c) Cone half-angle, 25° .(d) Cone half-angle, 30° .

Figure 7. - Concluded. Variation of theoretical additive drag of annular-nose inlet with conical flow at inlet.

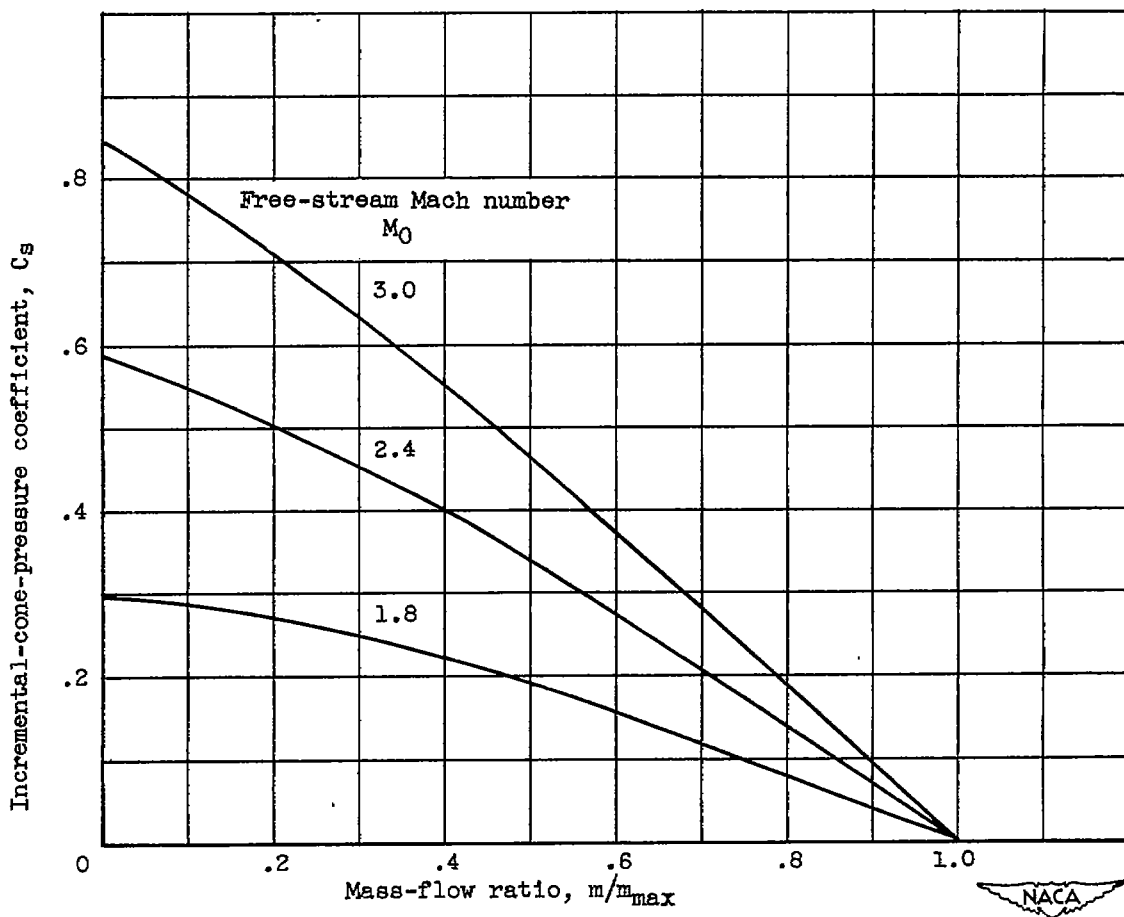
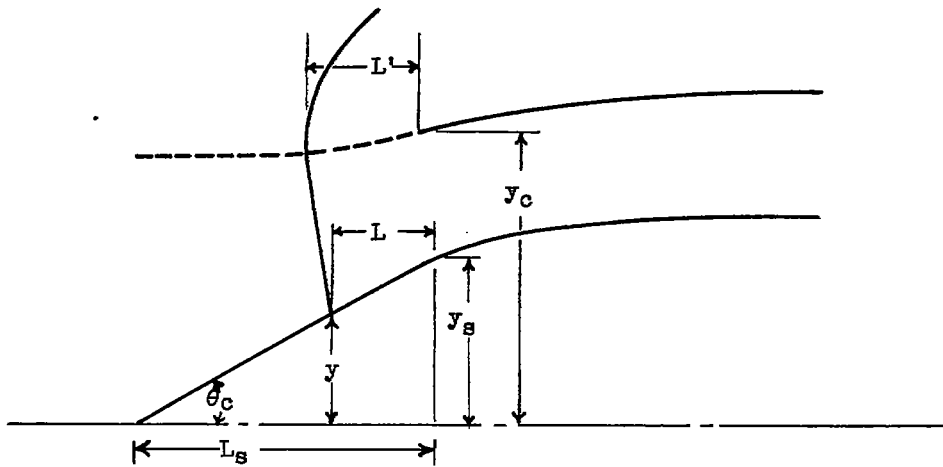


Figure 8. - Variation of incremental-cone-pressure coefficient with free-stream Mach number. Cone half-angle, 25° .

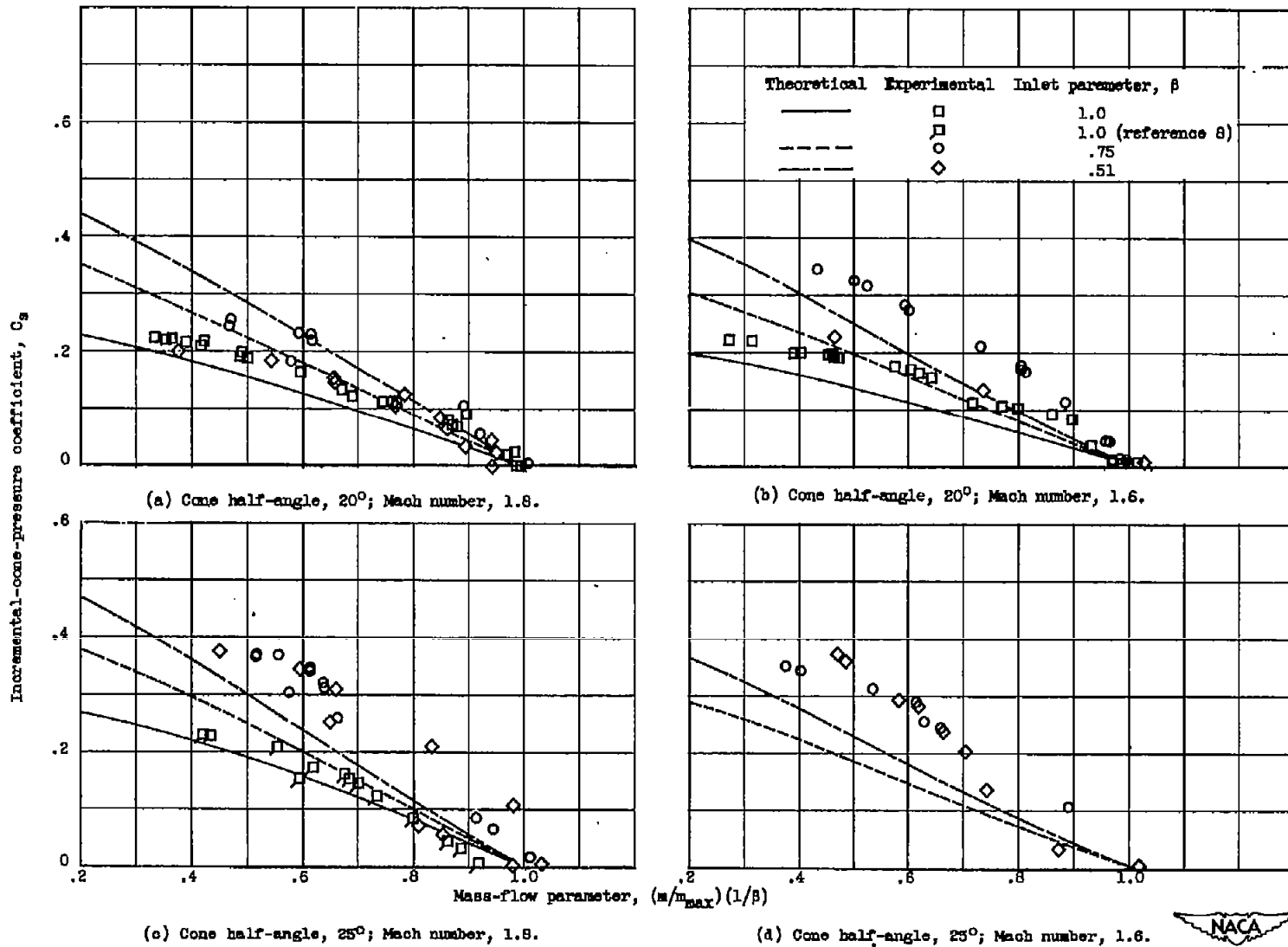
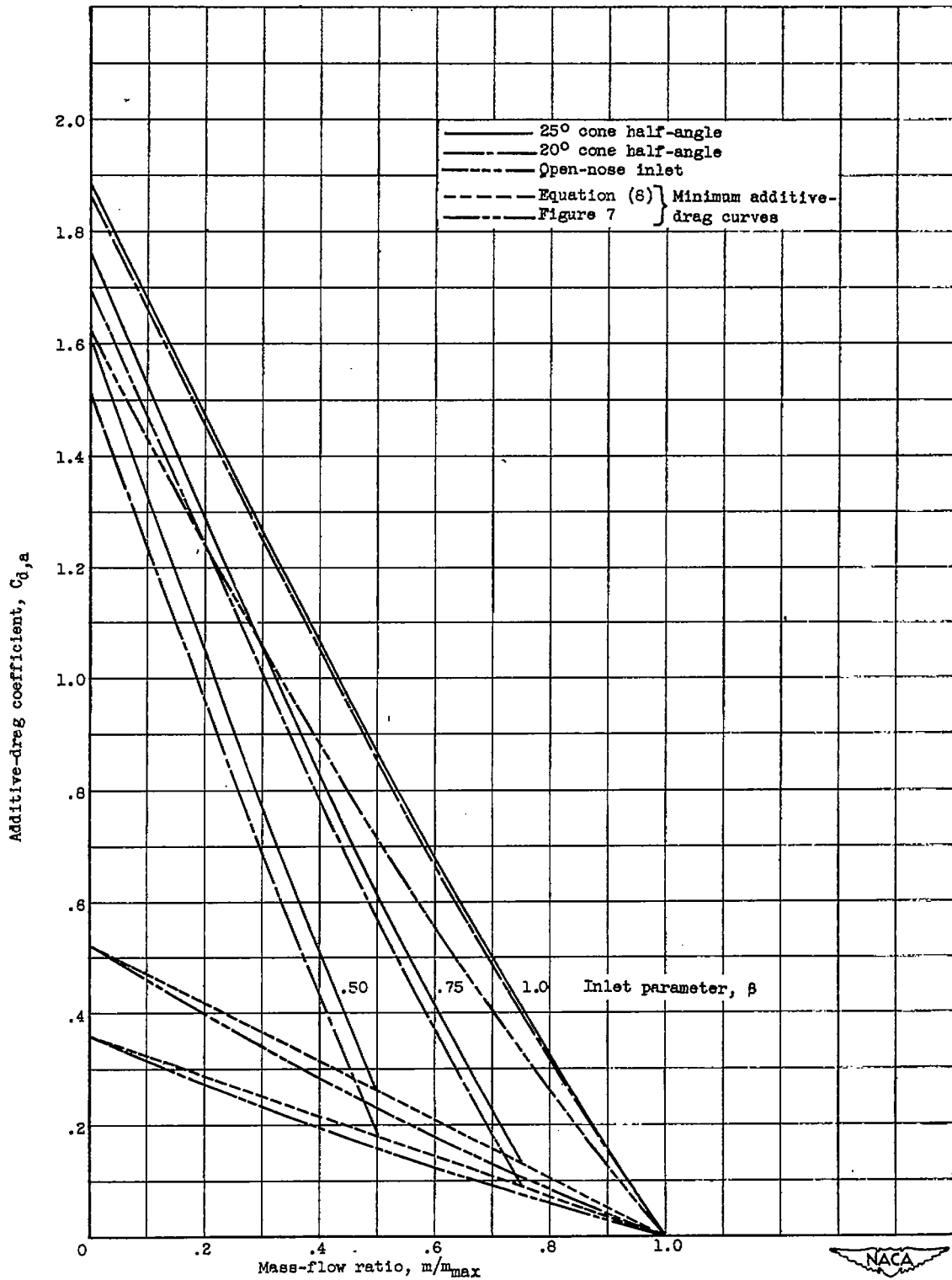


Figure 9. - Comparison of theoretical and experimental values of incremental-cone-pressure coefficient.



~~CONFIDENTIAL~~



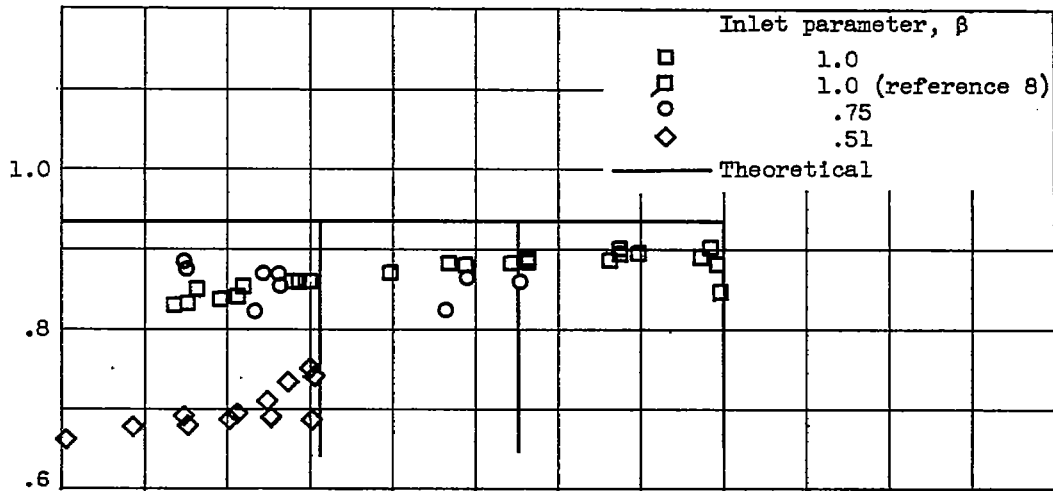
2119

Figure 10. - Effect of cone angle and inlet parameter β on additive drag. Mach number, 1.8.

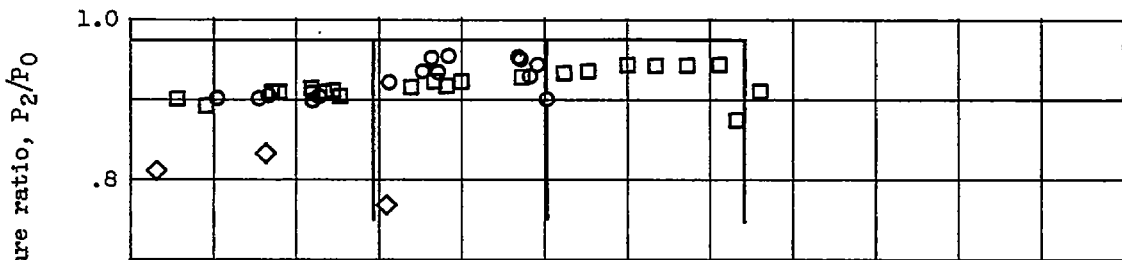
~~CONFIDENTIAL~~



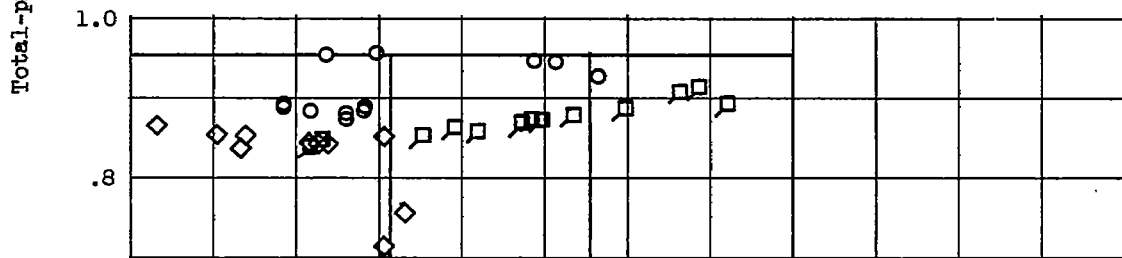
2119



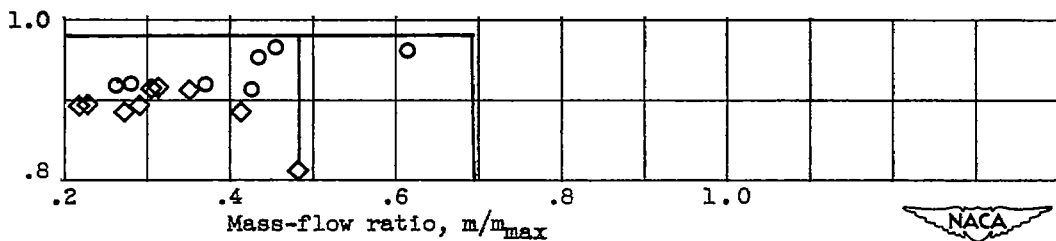
(a) Cone half-angle, 20° ; free-stream Mach number, 1.8.



(b) Cone half-angle, 20° ; free-stream Mach number, 1.6.



(c) Cone half-angle, 25° ; free-stream Mach number, 1.8.



(d) Cone half-angle, 25° ; free-stream Mach number, 1.6.

Figure 11. - Comparison of theoretical and experimental values of inlet total-pressure recovery.



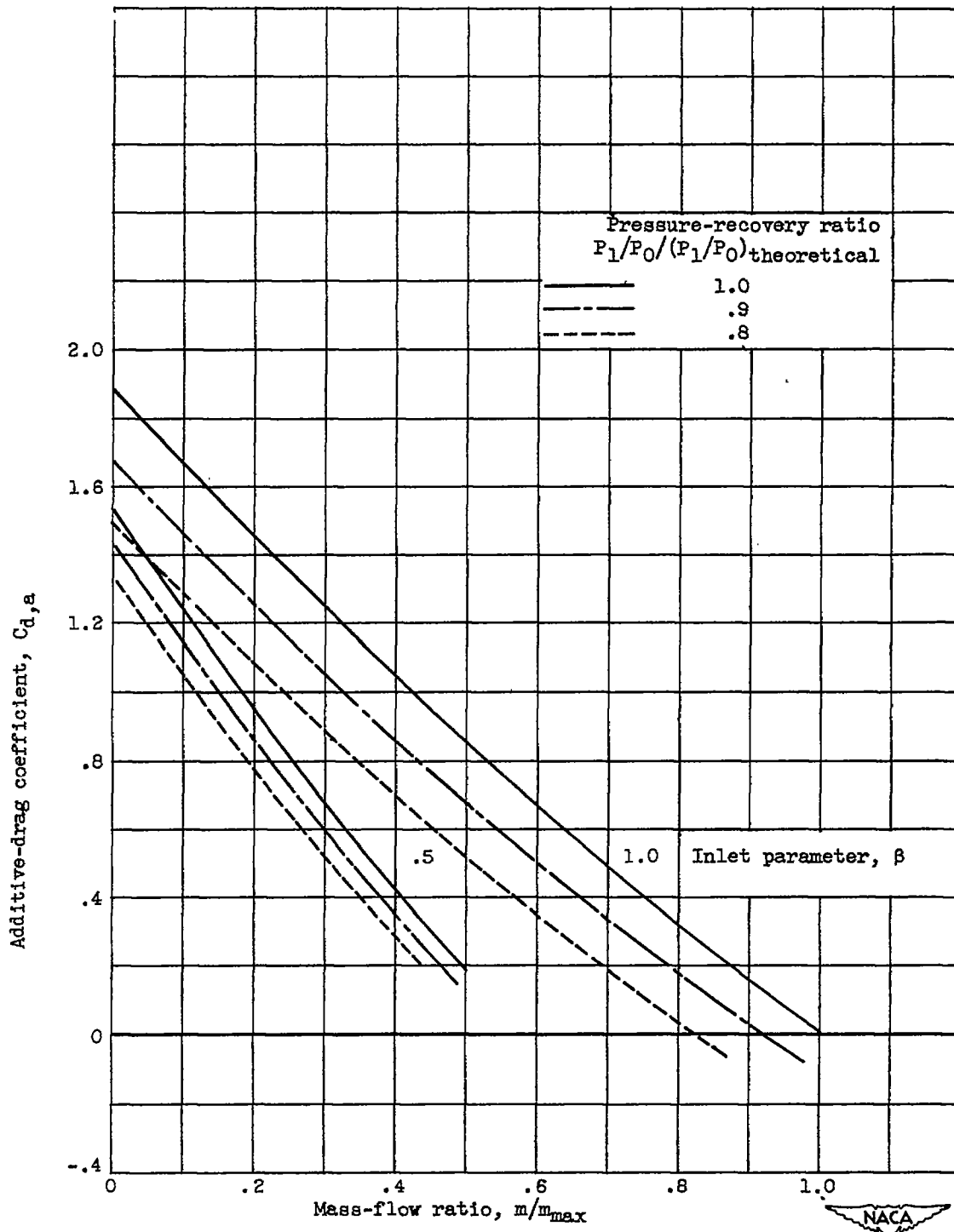


Figure 12. - Effect of inlet total-pressure recovery on additive drag.
Cone half-angle, 20° ; Mach number, 1.8.

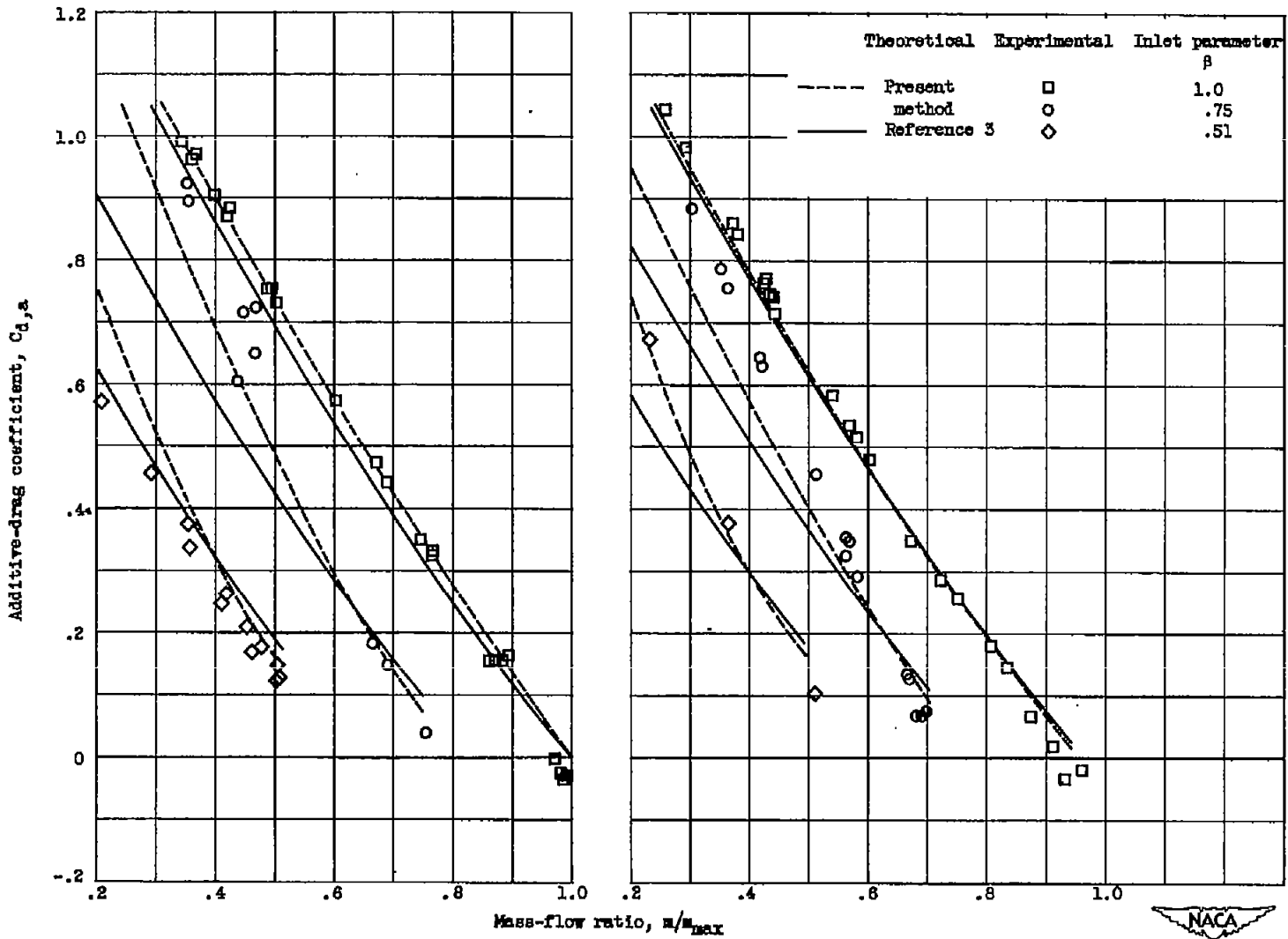
(a) Cone half-angle, 20° ; Mach number, 1.8.(b) Cone half-angle, 20° ; Mach number, 1.6.

Figure 13. - Comparison of theoretical and experimental variations of additive drag with mass-flow ratio for several center-body projections.

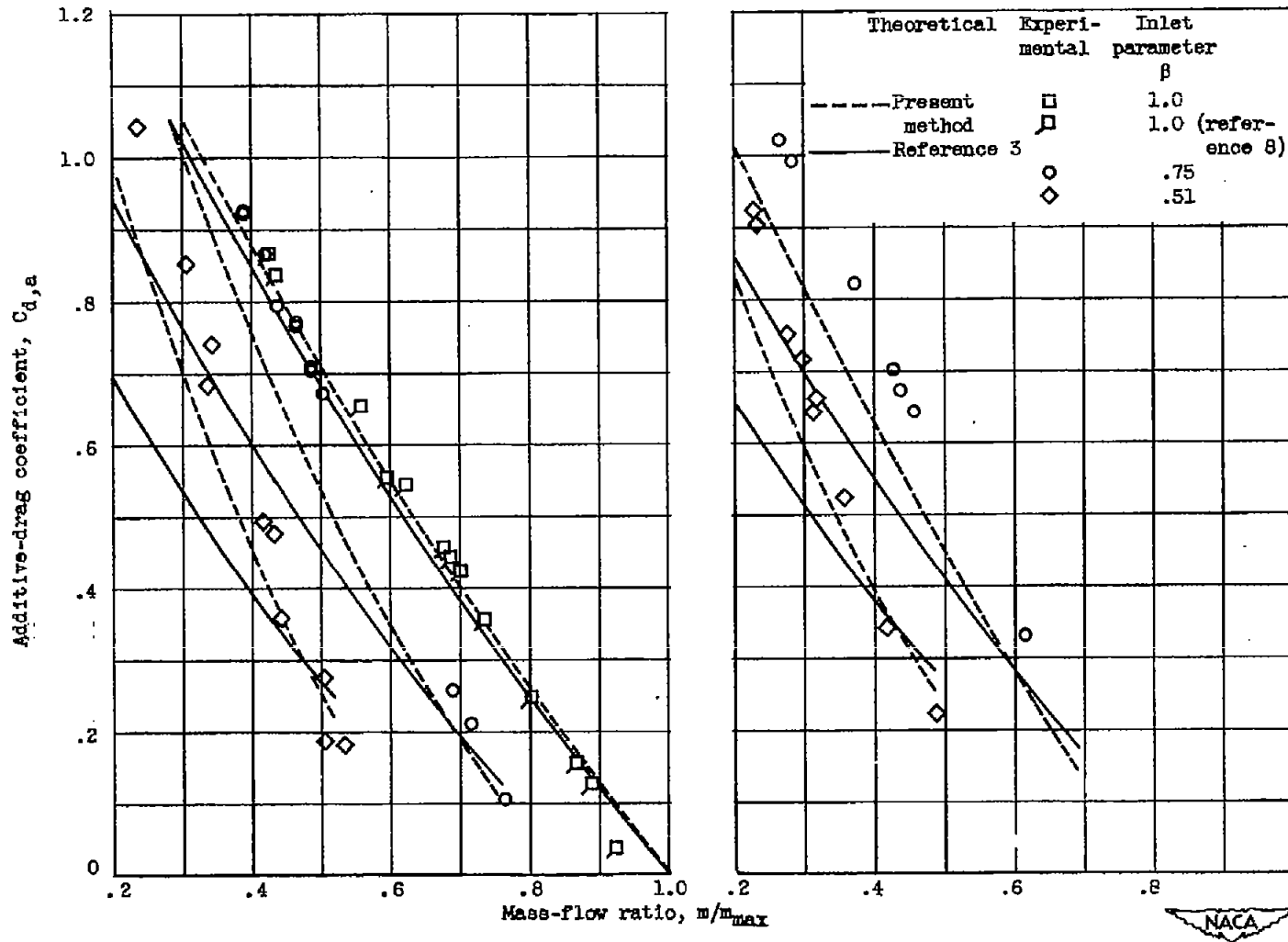
(c) Cone half-angle, 25° ; Mach number, 1.8.(d) Cone half-angle, 25° ; Mach number, 1.6.

Figure 13. - Concluded. Comparison of theoretical and experimental variations of additive drag with mass-flow ratio for several center-body projections.

